Morphing composite cylindrical lattices with enhanced bending stiffness

Materials & Design 222 (2022) 111056

Contents lists available at ScienceDirect

Materials & Design

journal homepage: www.elsevier.com/locate/matdes

Morphing composite cylindrical lattices with enhanced bending stiffness

Ciarán McHale *, Paul M. Weaver

Bernal Institute, University of Limerick, Castletroy, Limerick City, Ireland

HIGHLIGHTS

- A new configuration of the morphing composite lattice is developed to increase the bending stiffness of the structure.
- The new lattice uses additional composite strips mounted concentrically to the pre-existing strips on the same fasteners.
- The new lattice configuration is bend tested and compared to two lattices in a conventional strip configuration.
- Testing showed that that the new strip configuration is more mass and volume efficient than the conventional configuration.

GRAPHICAL ABSTRACT

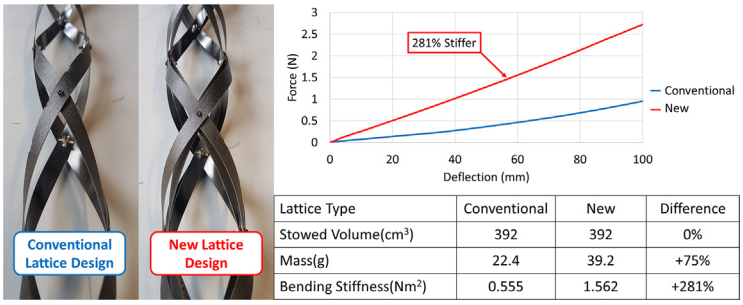

Lattice Type	Conventional	New	Difference
Stowed Volume(cm^3)	392	392	0%
Mass(g)	22.4	39.2	+75%
Bending Stiffness(Nm^2)	0.555	1.562	+281%

ARTICLE INFO

Article history:
Received 15 March 2022
Revised 15 July 2022
Accepted 11 August 2022
Available online 17 August 2022

Keywords:
Multi-stable
Morphing structures
Cylindrical lattice
Experimental testing

ABSTRACT

A key aspect in the design of deployable space structures comprising slender elements such as booms is their deployed bending stiffness. In space, due to zero gravitational loading, a high level of bending stiffness is not required to support neighbouring structures, but instead is desirable to resist vibrations generated by the attitude control system. The morphing composite cylindrical lattice that is under development is a structure with significant potential for deployable applications in space, however, concepts developed so far may lack sufficient bending stiffness. Therefore, current work focuses on developing a method of increasing the lattice bending stiffness, while minimising any increase in both mass and stowed volume. These goals are achieved by using additional composite strips mounted adjacent and concentric to pre-existing strips. These strips are attached using pre-existing fasteners, thus, only increasing the weight of the structure by the mass of the composite strips. A finite element model of the new lattice configuration is developed and validated by comparison to experimental results. For this comparison, three different lattice configurations were manufactured, two lattices with a conventional strip configuration, an eight-strip lattice and a four-strip lattice, and a third using a new lattice configuration developed in this work. In comparison with the eight-strip lattice, the new lattice configuration is 32% less stiff, however it weights 33% less and stows to approximately half the stowed height. Compared to the four-strip lattice, the new configuration weighs 75% more, but it is 281% stiffer while stowing to the same volume. By increasing the deployed bending stiffness, this work makes the morphing cylindrical lattice a more viable candidate for deployable space structures.

1. Introduction

Morphing, or multistable, structures are unique in their ability to change their shape or position while retaining structural stiff-

* Corresponding author.

https://doi.org/10.1016/j.matdes.2022.111056
0264-1275/

Nomenclature

Physical quantities

b	Width of the composite strip (mm)
d	Distance from the neutral plane to the centroid of the strip (mm)
h	Thickness of the composite strip (mm)
v_{12}	Poisson's Ratio
A	Area of strip cross section (mm^2)
E	Effective Young's modulus of the lattice (GPa)
E_{11}	Young's modulus in the fibre direction (GPa)
E_{22}	Young's modulus in the matrix direction (GPa)
EI	Bending stiffness (Nmm^2)
F	Force (N)
G_{12}	Shear modulus (GPa)
I	Effective second moment of area of the lattice (mm^4)
Ixx	Second moment of area (mm^4)
L	Length of the deployed lattice (mm)
SL	Strip length (mm)
SW	Strip width (mm)
δ	Deflection of the lattice (mm)
θ	Angle of rotation of the strip relative to the neutral plane (rad)
χ	Manufactured radius of the strips (mm)

Acronyms

ACW	Anti-clockwise
CFRP	Carbon fibre reinforced plastic
CTM	Collapsible tubular mast
CW	Clockwise
FE	Finite element
STEM	Storable tubular extendible member

ness in two or more configurations. An example of a commonly studied morphing structure is a bistable plate. This plate can be stable in two distinct shapes; where it is curved around one principal axis and then curved around an axis perpendicular to the first [1]. Multistability is achieved by tailoring and creating a structure with multiple potential energy minima [2]. Composite materials, such as carbon fibre reinforced polymers (CFRP), are often used in morphing structures, due to their high tailorability, stiffness and inherent lightweight [3]. These properties make morphing structures well-suited for deployable space applications, such as booms, solar arrays and antennae. Deployable space structures have the conflicting requirements of needing a small package for launch and a large length or surface area once deployed. Space deployables using morphing structures have the potential to be lighter and more packing efficient compared to structures relying on more traditional mechanisms, such as telescopic and articulated structures [4].

One of the most common types of morphing composite deployable is the Collapsible Tubular Mast (CTM) [5], a bistable deployable boom. This type of boom has a closed tubular cross-section that can be flattened and rolled to create a compact stowed package. Bistabilty in CTM booms is achieved by tailoring the manufacturing prestress and the stiffness properties of the composite. CTM booms have been utilised in many deployable structures [6 7]and have recently been proposed by NASA in the design of advanced solar sail technology for CubeSats on deep space missions [8]. Efforts have also been put into increasing the bending stiffness of the CTM boom by using corrugated thin shells [9]. In space, there is no air to dampen vibrations, so sufficient bending stiffness is required in deployable space structures to prevent damage [10]. A different type of bistable deployable boom is the Storable Tubular Extendible Member (STEM) [11]. Similar to the CTM booms, they can be flattened and rolled into a compact package, however the deployed cross section can vary in shape. The Roll-Out Solar Array utilised two STEM booms with a circular cross section to deploy solar panels and to provide stiffness to the structure [4 12]. Another STEM boom is the AstroTube, a lightweight composite tape spring that can deploy to 1.5 m from a 1U CubeSat stowed volume [13]. A variation of the tape spring design is the triangular rollable and collapsible boom, which is manufactured from two composite tapes bonded together to make a triangular shape [14]. In the extended state, the triangular cross-section of the boom provides increased bending stiffness compared to a single tape. A different type of morphing composite structure with great potential in space deployables is the multistable composite cylindrical lattice [15].

The multistable lattice is a shape-changing structure that can morph from a long, deployed state to a short, stowed state and vice versa. The morphing lattice comprises clockwise and anticlockwise helical strips of CFRP bound together with metal fasteners to a cylindrical shape. The cylindrical lattice is a multistable structure that can be tailored to be stable at multiple positions along the lattice length. The lattice attains its multistability through the exploitation of the interplay between the prestress, material properties and structural geometry. The composite strips are prestressed by first curing them on a curved mould of a particular radius and twist. Post-cure, the composite strips are assembled into intersecting helices and constrained to the smaller radius of the lattice structure, creating prestress. In prior work, the analytical model of the lattice was developed to accurately predict the stability characteristics of the structure through the calculation of the bending curvatures, membrane strains [16], and thermal residual stresses [17]. This analytical model facilitated the development of a deployable space boom that utilised multiple morphing lattices.

The lattice boom consists of two morphing composite lattices that are connected telescopically and that store by nesting within one another in the stowed state [18]. This configuration greatly increases the deployed length of the structure while maintaining the same stowed volume of a single lattice. The two lattices in the boom were designed to be self-deploying and therefore required an internally stored motor to control the speed of deployment. In the stowed state the lattice boom has the volume of a 1U CubeSat and in the deployed state it has a length of over 2 m, making it highly packing efficient. However, this structure had one significant shortcoming, a relatively low bending stiffness. Space booms require adequate bending stiffness to resist vibrations from the attitude control system to prevent damage to the boom and its attached devices [10]. Additionally, a low level of bending stiffness can adversely affect the deployment of the morphing lattice when using a deployment speed regulator [18]. Mid-deployment, the lattice boom temporarily buckled to one side under its own deployment force, due to its relatively low bending stiffness, Fig. 1. This behaviour is highly undesirable as the lateral deployment of the boom may cause damage to other components of a satellite and prevent multiple booms from being used in series, for example, in a solar array. Therefore, the purpose of current work is to develop a method of efficiently increasing the bending stiffness

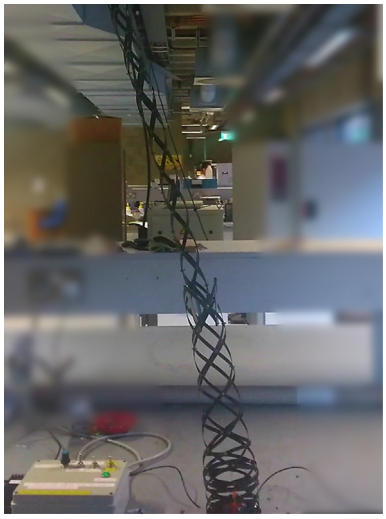

Fig. 1. Lattice boom mid deployment buckling under its own deployment force [18].

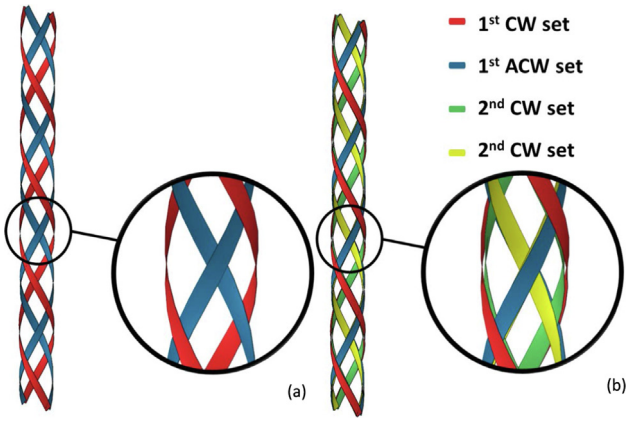

Fig. 2. Comparison of conventional and new lattices (a) Conventional four-strip lattice in the deployed state (b) New eight strip lattice in the deployed state. Note, the first set of clockwise (CW) and anti-clockwise strips (ACW) are depicted in red and blue respectively and the second set of clockwise and anti-clockwise strips are depicted in green and yellow, respectively. (For interpretation of the references to colour in this figure legend, the reader is referred to the web version of this article.)

of the morphing lattice and so make it a more viable option in the design of space deployable structures.

A simple method of increasing the bending stiffness involves using additional layers in the composite laminate of the lattice strips. More layers significantly increases the bending stiffness of the structure, however, too many layers can make the strips too stiff to be assembled into the lattice shape. In previous work on the lattice boom [18], it was discovered that five layers was the limit for the particular lattice configurations used in the boom. Using six layers in the lattice strips resulted in them exceeding their breaking strain during assembly. Another method to increase the bending stiffness is by increasing the width of the composite strips. However, increasing the strip width would result in a similar increase in the stowed height of the lattice, e.g., increasing the strip width by 50 % would also increase the stowed height by 50 %. Increasing the number of composite strips in the lattice has a similar issue as the stowed volume also increases. Additionally, using more strips significantly increases the weight of the structure as more fasteners are required for assembly.

The solution proposed herein is to use additional sets of strips adjacent to and concentric to existing strips, attached with pre-existing fasteners. In lattice configurations, there is generally-one set of strips configured in a clockwise helix and one set of strips configured in an anti-clockwise helix. Henceforth, this type of lattice is referred to as the conventional lattice configuration. The proposed new lattice configuration simply uses additional sets of clockwise and anti-clockwise helical strips connected in parallel (i.e., concentrically) and inside of the existing sets. This type of lattice is referred to as the new lattice configuration. The differences in the composite strip layout between the conventional and new lattice configurations are shown in Fig. 2. As the new strips are mounted inside, the stowed volume of the structure does not change. Additionally, as the existing fasteners are being used, the mass of the structure only increases by the weight of the composite strips. The stiffness of this new lattice configuration is evaluated herein through finite element modelling and experimental testing. This new lattice is then compared with two lattices that use the conventional lattice configuration, one with the same number of strips and the second with the same stowed volume, to determine the stowage, mass, and stiffness benefits of the new configuration.

This paper is structured as follows. Section 2 starts with a short description of the morphing lattice, followed by the introduction of some key expressions used to analyse its bending stiffness. In Section 3, a finite element model of the lattice is developed, detailing the steps from prestressing the strips to bending of the full structure. Section 4 describes the manufacture of three different lattice configurations and the method of testing. In Section 5, the results from the numerical and experimental models are compared and discussed. Finally, conclusions are drawn in Section 6.

2. Model

2.1. Description of the lattice

The morphing composite lattice comprises multiple narrow composite strips that follow clockwise and anti-clockwise helical paths around the cylindrical shape of the lattice. The strips are bound to this shape with mechanical fasteners at discrete locations. These composite strips are first cured in an autoclave at an elevated temperature and pressure. Prestress in the strips is created by curing the strips on a curved mould of a particular radius. Post-cure, after cooldown, the strips are constrained to the smaller radius of the lattice, generating prestress in the longitudinal and twist directions. Current work concerns lattices that utilise a symmetrical laminate configuration in the strips. This type of laminate is utilised to simplify the modelling of the lattice, avoiding significant thermal warping. Non-symmetrical laminates cured at an elevated temperature produce thermal residual stresses in the post-cure cooldown that can result in large thermal warps. Thermal warping of the strips has a significant influence on the stability characteristics of the lattice and complicates modelling.

2.2. Second moment of area

The second moment of area, I_{xx}, of the lattice configurations analysed herein is calculated to determine the stiffnesses of the strip configurations. The strips of the lattice follow a helical path, changing the cross-sectional area of the lattice along its length. At any one point along the lattice, the cross-section is made up of rectangles (i.e., the strips) positioned around the radius of the lattice. Therefore, the expression for the second moment of area of a rotated rectangle is used, [19].

$$I_{xx} = \frac{bh}{12}\left(b^2 cos^2\theta + h^2 sin^2\theta\right) + Ad^2 \quad (1)$$

where b is the width of the composite strip, h is the thickness of the strip, θ is the angle of rotation of the strip relative to the neutral plane of the lattice, A is the area of the strip and d is the distance from the neutral plane of the lattice to the centroid of the strip. From Eq. (1), the second moment of area of each of the individual strips can be calculated and summed together. By repeating this calculation at periodic increments along the lattice length, the change in the second moment of area can be evaluated.

2.3. Bending stiffness calculation

A series of cantilever beam tests with a point load on end is performed on three lattices in Section 4. The bending stiffness, EI, of the lattices can be experimentally calculated using the simple expression for the deflection of an end-loaded cantilever, given by [20].

$$EI = \frac{FL^3}{3\delta} \tag{2}$$

where E is the effective Young's modulus of the lattice, I is the overall second moment of area of the lattice, obtained from averaging I_{xx} along the lattice length, F is the experimentally recorded force, L is the length of the deployed lattice and δ is the recorded deflection of the lattice.

3. Finite element analysis

To analyse the bending stiffness of the composite cylindrical lattice, a numerical model was developed using Abaqus/CAE [21]. Three different lattice models were developed to calculate the bending stiffness of each of the different lattice types. Two of the models are of lattices with conventional configurations and one uses the new lattice configuration. The details of the three lattices are found in Table 1. All of the strips in the lattices use the same material and composite layup of [0/90/0] and have the same pre-curvature of 400 mm in radius, making the number of strips and their configurations the only difference between the lattice models. This particular laminate configuration and pre-curvature was selected as previous work [16] showed that it produced a lattice stable in the deployed state. The material used in these lattices is IM7 8552 unidirectional prepreg composite, the properties of which can be found in Table 2. Previous work on the lattice determined that reduced four-node shell elements (S4R) of 1 mm^2 in cross-sectional area were suitable for analysing the structure [18]. Analysis of each of the lattices was split into two separate models, assembly and bending. In the first model, the lattice strips are prestressed and assembled into a deployed lattice, and in the second model, the bending analysis is performed. All models use a Newton-Raphson nonlinear solution in their analysis.

3.1. Lattice assembly

The lattice with the new strip configuration is used to exemplify the methodology used for all three lattice models. Initially, the lattice strips are created as shell extrusions in their cured radius of 400 mm. As a symmetrical layup is used, thermal effects derived from the post-cure cooldown are ignored to simplify the analysis. In the initial step, the strips are co-located around the centre of the lattice. A boundary condition is applied to a centre line along the length of the strips to prevent them from moving in the z-axis and rotating about the x and y axes during the prestressing step. Next, the strips are moved into their positions on the lattice by applying a displacement in the y-axis to the midpoint of each of the strips, Fig. 3 (a). Concurrently, a z-rotation is applied to either end of each strip, coiling them into the smaller radius of the lattice. Fig. 3 (b) shows the lattices strips after the prestressing step, coiled to the radius of the lattice in the stowed state.

fter prestressing, the strips can be deployed from the stowed state to the extended state. First, the fasteners of the lattice are simulated using specific boundary conditions in Abaqus, as achieved by placing boundary conditions where the strips intersect in the extended state. The type of boundary condition varies depending on its position in the lattice. The boundary conditions on the y-axis prevent rotation about the z-axis and x-displacements, and the boundary conditions on the x-axis prevent rotation about the z-axis and y displacements, see Fig. 4(a). Next, one end of each strip is restricted with a zero displacement in the z-direction and the opposite end is given a displacement of 560 mm in the z-direction, representing the stable length of the lattice. Fig. 4 (b) shows the boundary conditions used in the lattice model at mid-deployment. Note, the conventional lattices are given a displacement of 580 mm as they have a slightly longer stable length. An additional displacement boundary condition of 280 mm was used at the midpoint of each strip to aid in the deployment. A damping factor of magnitude 2×10^{-7} was used to numerically stabilize the analysis in this step. At the end of this step, the lattice resides in its stable, deployed shape, ready for bending, Fig. 5.

3.2. Lattice bending

To enable overall bending of the lattice, the lattice strips have to be exported to a new model, as the fasteners cannot be simulated with boundary conditions as was done in the deployment analysis. To achieve this behaviour, the mesh of the deployed lattice is imported into the second model. Then, the stresses and strains of the deployed lattice are extracted and applied to the strips using an initial state predefined field. Coupling constraints are used to simulate the lattice fasteners by binding the nodes of the strips at the fastener locations together in the x-, y- and z- directions, while leaving all rotations free. Frictionless surface-to-surface contacts are used to simulate the interactions between the lattice strips. Friction surface-to-surface contacts between the strips was attempted but doing so resulted in the simulation failing to converge. The contacts are used in this model to prevent the strips from interpenetrating during the bending simulation. An increase in bending stiffness was observed in the lattices when including the contacts compared to the models without them. A cantilever bend test was simulated to assess the bending stiffness of the lattices. Encastre boundary conditions were applied to one end of each of the lattice strips. At the opposite end of the lattice, a 3 N load in the y-direction was applied to the end of a single strip, simulating the experimental testing conditions, Fig. 6. After the simulation was completed, the deflection and load on the lattice were

Table 1
Lattice configuration details.

Lattice	Material	No. of Strips	Config Type	Lay-up (°)	χ (mm)	SL (mm)	SW (mm)	Revolutions
Config 1	IM7 8552	4	Conventional	[0/90/0]	400	630	10	2
Config 2	IM7 8552	8	Conventional	[0/90/0]	400	630	10	2
Config 3	IM7 8552	8	New	[0/90/0]	400	630	10	2

Table 2
Material Properties.

Material	E_{11} (GPa)	E_{22} (GPa)	G_{12} (GPa)	ν_{12} (–)	Ply Thickness (mm)
IM78552 [22]	161	11.4	5.2	0.32	0.125*

*Measured.

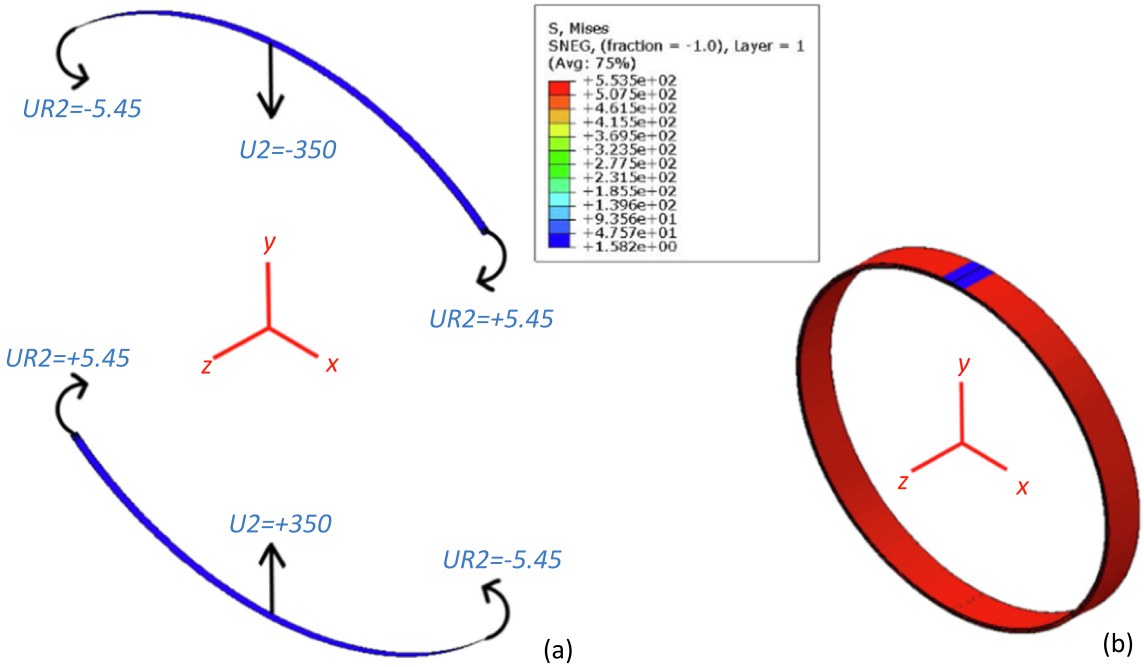

Fig. 3. The strips are coiled into a smaller radius using rotation boundary conditions at the strip ends and a displacement at the midpoint (a). The strips mechanically prestressed in the stowed configuration (b).

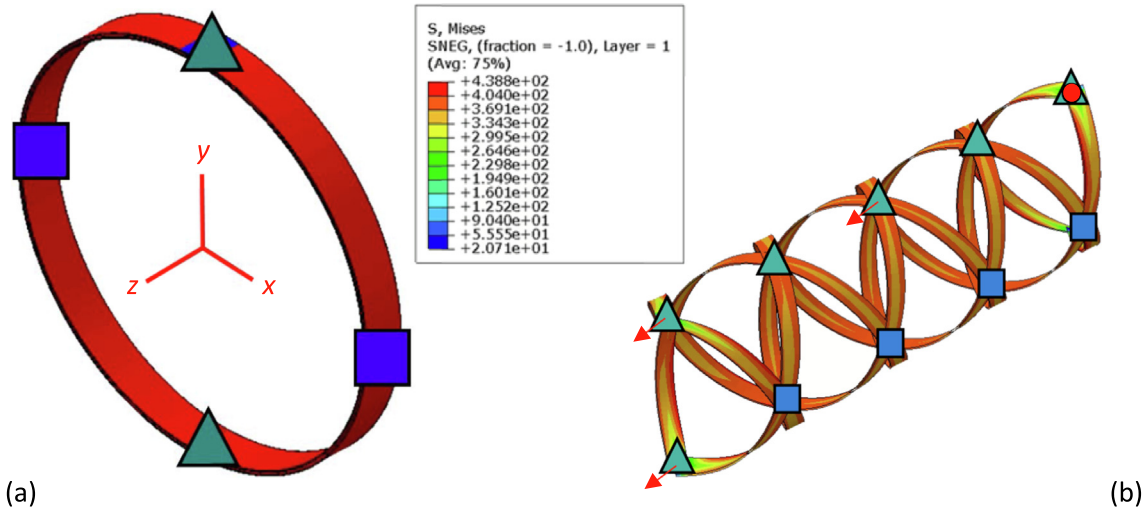

Fig. 4. Locations of fastener boundary conditions. Blue squares are locked in y- displacement and z- rotation and green triangles are locked in x- displacement and z- rotation (a). The new lattice configuration in a semi-deployed state. Red arrows represent the z- displacements used to deploy the lattice and the red circles represents the location of the zero z- displacement boundary conditions (b). (For interpretation of the references to colour in this figure legend, the reader is referred to the web version of this article.)

recorded for comparison with the experimental tests to validate the developed model. This process was repeated for the two lattices with the conventional strip configuration. The PC used in the finite element modelling used an Intel i3 6300 processor with 8GBs of RAM. The computational time for all three lattice configurations for both the deployment and bending models is shown in Table 3. The finite element models for the lattices with eight strips take more than twice as long to compute than the lattice with just four strips. The bending model of the new eight strip lattice configuration takes over two minutes longer than the conventional eight strip lattice as there is more contact points between the strips, increasing computational complexity.

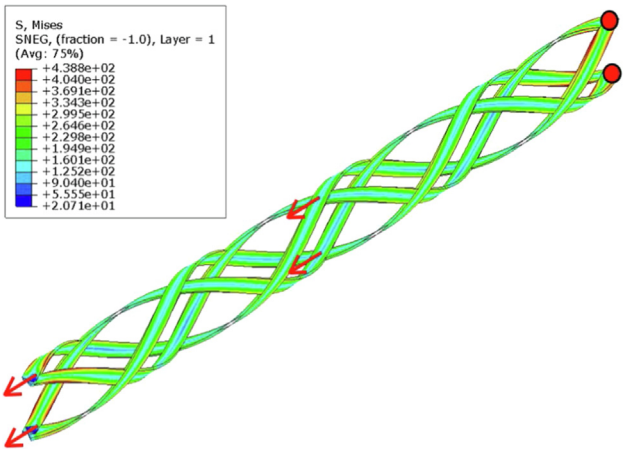

Fig. 5. The new lattice configuration in the deployed state. Red arrows represent the z- displacements used to deploy the lattice and the red circles represents the location of the zero z- displacement boundary conditions. (For interpretation of the references to colour in this figure legend, the reader is referred to the web version of this article.)

4. Experimentation

4.1. Manufacture

Three different lattice configurations were manufactured and tested to validate the developed numerical model of the new lattice configuration. Two of the lattices use a conventional lattice configuration of two sets of strips and the last uses the new lattice configuration with four sets of strips, Table 1. To ensure consistency of material properties and pre-curvature, the strips of all three lattices were cut from a single panel. The material used in this panel was IM7 8552, a unidirectional prepreg composite, Table 2. This panel was cured on a curved mould of 400 mm in radius to produce the desired prestress when assembled into the lattice shape. During the layup process, a peel ply layer was not used, instead, release film was used on either side of the composite laminate. This produces a smooth, resin-filled surface, that reduces friction in the deployment of the lattice. To cure the panel, it was placed in an autoclave at 180 °C and 6.5 bar pressure, with a dwell time of two hours. As a symmetrical lay-up was used, no significant thermal warping was observed in the panel on removal from the mould. Next, the composite panel was cut into twenty 10 mm strips using a water jet cutter at low pressure. The hole spacing for the fasteners was determined using a computer aided design model, with each set of strips having slightly different spacings due to their different radial positions in the lattice. With the holes drilled, the composite strips were assembled into three lattices with 2 mm bolts and locknuts. Washers were used between each strip to reduce friction in deployment. As a result, the new lattice configuration required three washers at each fastener location.

Fig. 7 shows the three assembled lattices in their deployed states. Both of the conventional lattices are stable at a deployed length of 580 mm, while the new lattice configuration is stable at a slightly shorter 560 mm. This difference in stable lengths is caused by the innermost set of strips in the new configuration being shorter than the outer strips, influencing the stable position and retracting the deployed length of the lattice by 20 mm. It is also observed that the new lattice configuration has a slightly larger stable radius than the two conventional lattices. Fig. 8 shows the three lattice configurations in their stowed states. In this state, the four-strip lattice and the new lattice configuration match in height, while the eight-strip lattice has nearly twice their stowed height. This comparison demonstrates the benefit of the new lattice design, as both the conventional eight-strip lattice and the new lattice configuration use the same number of composite strips, but one stows to nearly half the height of the other. Fig. 9 shows a close up view of the different sets of clockwise and anti-clockwise strips in the new lattice assembly, with four strips overlapping each other at each fastener location.

4.2. Bend testing

A series of cantilever bend tests with a point load at one end was used to evaluate the bending stiffness of the three assembled lattices. In prior studies [18], a simply supported beam with a central point load experiment was used to assess the bending stiffness of the lattice. This experimental set-up was not repeated here as the central point load caused the lattices to initially change their diameters before bending. In these studies, the initial radius of the tested lattices was narrow and only changed by an insignificant amount before bending occurred. However, the lattices produced in the current study are larger in diameter, causing this initial morphing response to prevent useful results from being obtained. With these considerations, an end-loaded cantilever bend test was used to prevent undesirable significant deformation of the lattice during experimental testing. Fig. 10 shows the experimental setup for this test. On the left, the lattice is fixed to an upright support, emulating the encastre boundary conditions of the finite element model. A 3D printed fixture (in white) is used to connect the strips of the lattices to the support. On the right, the lattice is connected to a

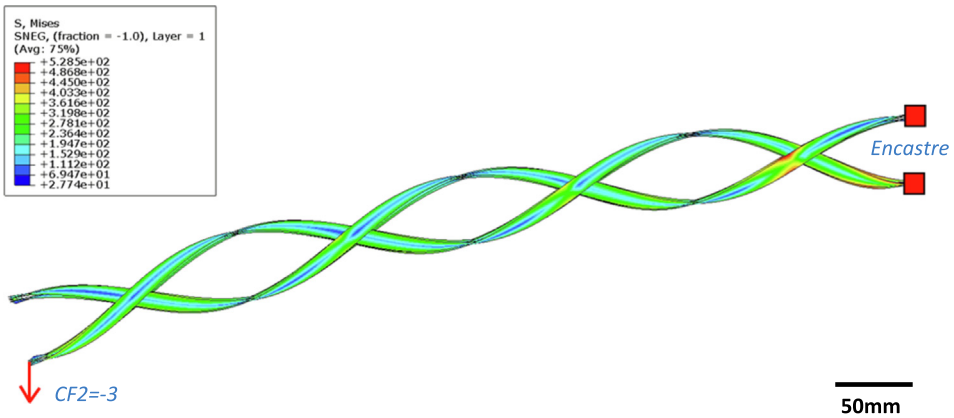

Fig. 6. Lattice with the new strip configuration deflecting to 100 mm under a load of approximately 2.5 N. Red squares represent the Encastre boundary condition, and the red arrow represents the applied load. (For interpretation of the references to colour in this figure legend, the reader is referred to the web version of this article.)

Table 3
Computational time for the finite element analysis models.

Lattice Configuration	Deployment Model (mins)	Bending Model (mins)
Conventional Four Strip	18:30	21
Conventional Eight Strip	37	49:30
New Eight Strip	38	53

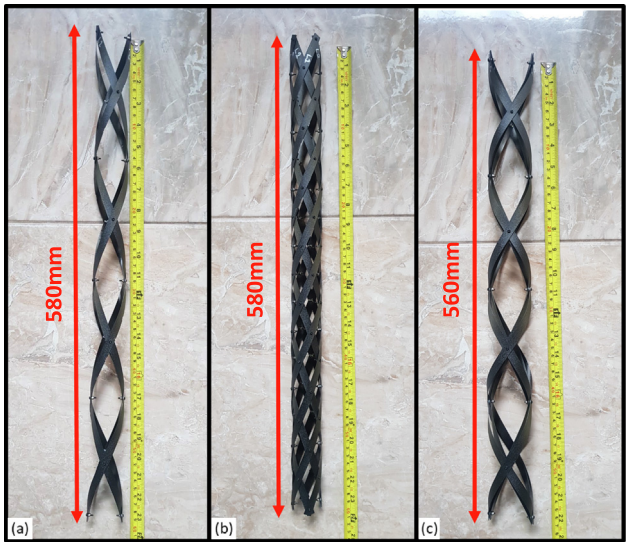

Fig. 7. The three lattice configurations in the deployed state, four-strip lattice (a), eight-strip lattice (b), new lattice configuration (c).

Tinius Olsen tensile tester with a cable to apply the load to the lattice in a upwards direction. Usually, wood would not be considered as a suitable material for a test frame, however, as the lattices are highly flexible, and the loads are low (1–4 N), it provides a sufficiently stiff and robust structure for these experiments. In this experiment, the lattice configuration is initially located in a neutral position and then the load is applied by the Tinius Olsen tensile tester. A 100 N load cell was fitted to the tester to record the force applied to the lattices. The deflection of the lattices was recorded by the displacement of the tensile tester cross-head. The force and deflection of the lattices are continually recorded during testing. Two different mounting configurations were tested with the conventional eight-strip lattice, mounting with only the top and bottom of the lattice ends secured and mounting with all four ends of the lattice secured. Both configurations were tested to observe the effect that the additional mounting points have on the bending stiffness. A maximum displacement of 100 mm was used to prevent any damage or plastic deformation in the lattices. To ensure consistency in the results, each lattice was tested four or five times.

Fig. 9. Close up of the additional strips used in the new lattice configuration. The added strips are mounted concentrically to the existing strips on the same fasteners.

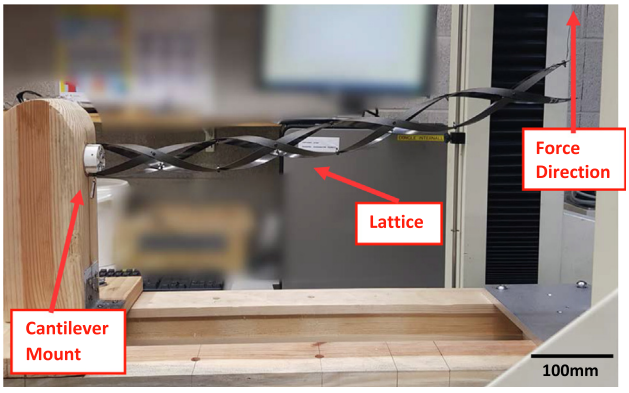

Fig. 10. Cantilever beam test of the four strip lattice. On the left, the lattice is securely mounted to the test frame and on the right, the load is applied to the lattice in an upwards direction.

5. Results & discussion

To evaluate the differences between the conventional lattice configuration and the new configuration, the second moment of

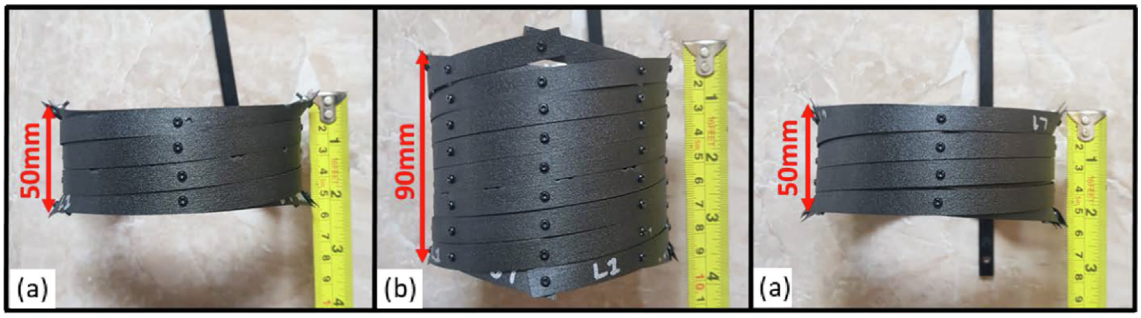

Fig. 8. The three lattice configurations in the stowed state, four-strip lattice (a), eight-strip lattice (b), new lattice configuration (c).

area, mass breakdown and force/deflection response of the three analysed lattices are discussed with relation to Fig. 11 to 14. First, the second moment of area of the lattices is calculated periodically along their lengths. Next, the lattices are compared in terms of the mass of the composite strips and mechanical fasteners. Finally, lattice test results are analysed and compared with the finite element models. The four experiments are then compared to each other to determine the advantages and disadvantages of the new type of lattice.

5.1. Second moment of area of lattice

The second moment of area (I_{xx}) of each lattice was calculated at periodic increments along their lengths using Eq. (1). Fig. 11 shows the variation of I_{xx} along the first half revolution of each of the lattices, after which its values repeat. For the conventional lattice, half a revolution represents a length of 145 mm, and for the slightly shorter new lattice configuration, its length is 140 mm. The I_{xx} for both the four-strip lattice and the new lattice configuration display a sinusoidal variation as the strips deploy along their helical path, changing position from the top and bottom of the lattice, to the sides, and then back again. The new lattice configuration displays nearly twice the I_{xx} of the four-strip lattice as it uses twice the number of strips in approximately the same positions. The conventional eight-strip lattice has a constant I_{xx} along the lattice length. As the strips revolve around the lattice, they swap relative positions. The strips that start in the top and bottom positions deploy to the sides and the strips that start in the side positions deploy to the top and bottom, creating a constant I_{xx}.

5.2. Mass breakdown

The mass of the strips and fasteners of each of the three lattices are detailed in Table 4. The strips in the new lattice configuration are slightly lighter than in the conventional eight-strip lattice as the inner strips are shorter. As the conventional eight-strip lattice has more fasteners than the other two lattices, its fastener weight is three to four times heavier. This effect results in over half of the mass of the conventional eight-strip lattice being attributed to the fasteners, whereas only a quarter of the mass of the new lattice configuration arises from fasteners. The mass of fasteners in the new lattice configuration is greater than the conventional four-strip lattice as it uses three washers at every fastener location to reduce friction between the strips. The mass benefits of the new lattice configuration can be determined by using the conventional four-strip lattice as a baseline and comparing the other two lattices to it. The new lattice configuration is 73 % heavier than the four-strip lattice, while using double the number of composite strips.

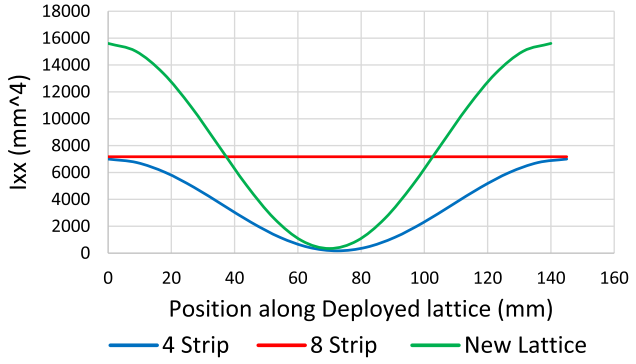

Fig. 11. Second moment of area of each of the lattice configurations over the first half revolution of the structure, after which the values repeat.

Table 4
Mass breakdown of the evaluated three lattices.

Parameter Mass	4 Strips	8 Strips	New 8 Strips
Strip	14.5 g	29.1 g	28.6 g
Fastener	7.9 g	29.8 g	10.1 g
Strip %	64.7 %	49.3 %	73.9 %
Fastener %	35.3 %	50.7 %	26.1 %
Total	22.4 g	58.9 g	38.7 g
Increase in Mass	0 %	163 %	73 %

The conventional eight-strip lattice also uses twice the number of strips, but it is 163 % heavier, largely due to the additional fasteners.

5.3. Force deflection response

The force/deflection responses of both four-strip and eight-strip conventional lattices with all mounting points secured are shown in Fig. 12. All experimental tests are included in the plot to demonstrate the consistency of the testing method, with the average shown in black. Starting with the four-strip lattice, Fig. 12(a), the tip deflection increases with the force displaying a non-linear response, with a slightly stiffening (concave up) path. Poor correlation is observed between the experiments and finite element (FE) model. While the results are similar, the FE model displays a slightly softening (convex) response. This difference is likely due to the frictionless contacts used between the strips in the FE model allowing it to deploy slightly rather than bend. This behaviour is not present in the experimental tests as the finite friction at the fasteners holds it in the stable position. From this plot, we can determine that the four-strip lattice is highly flexible, as less than 1 N is required to deflect the lattice to 100 mm. This flexibility demonstrates the necessity of increasing the bending stiffness of the morphing lattice for use in space applications. By doubling the number of strips in the lattice, Fig. 12(b), the stiffness increases significantly. For this set of results, the lattice is securely mounted to the test frame, with all four ends. The force/deflection response in this lattice is more linear than the four-strip lattice and it is four times stiffer, requiring 4 N to deflect 100 mm. This significant increase in stiffness is caused by the difference in the second moment of area of the lattice cross-section. The second moment of area of the four-strip lattice varies sinusoidally along its length, changing from being relatively high to low as the strips revolve around the lattice. However, in the eight-strip lattice, the additional strips balance out the second moment of area along the length, creating a constant second moment of area. Better correlation is observed with the FE model for this lattice, that is likely due to the increased bending stiffness of the lattice dominating over friction effects at the fasteners.

The force/deflection responses of the conventional eight-strip lattice with only two ends secured and the new eight-strip lattice configuration are shown in Fig. 13. By using only two mounting points, the stiffness of the eight-strip lattice significantly decreases, requiring only 2.5 N to deflect to 100 mm. During testing, the two unsecured ends of the lattice flared out, allowing the lattice to deform more easily, resulting in reduced stiffness. Again, good correlation with the FE model is shown with the stiffer lattice. Fig. 13 (b) shows the response of the new lattice configuration, where some variance in the experimental results is observed, but in general, are relatively consistent. The force/deployment response of this lattice is similar to the previous lattice, deflecting to 100 mm under a 2.5–3 N load. This response happens because both lattices have the same number of composite strips under the same mounting conditions. Good correlation is shown again between the experimental results and FE model for this lattice configuration.

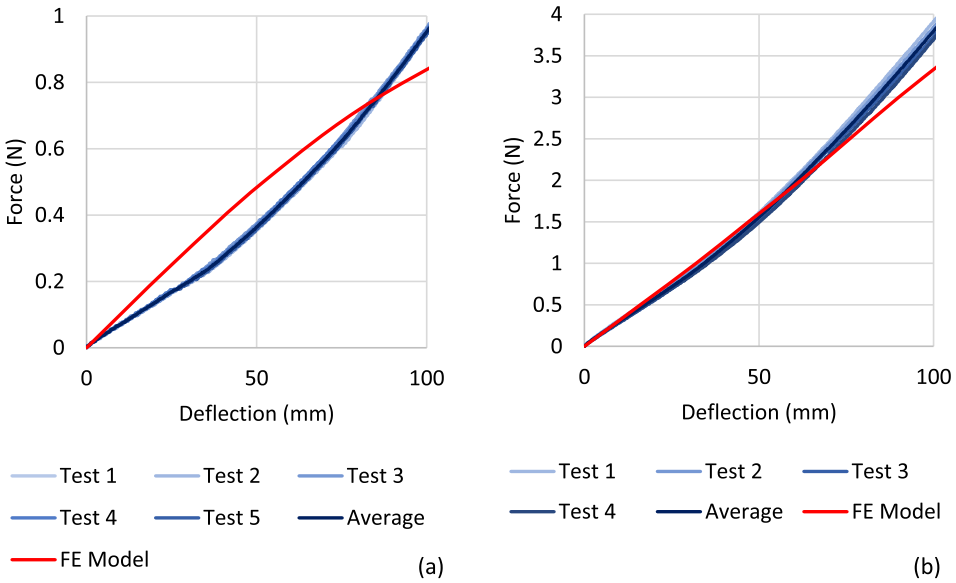

Fig 12. Force/Deflection plot of the four strip lattice, comparing the experimental tests to the finite element model (a), Force/ Deflection plot of the eight-strip lattice utilising all 4 mounting points (b).

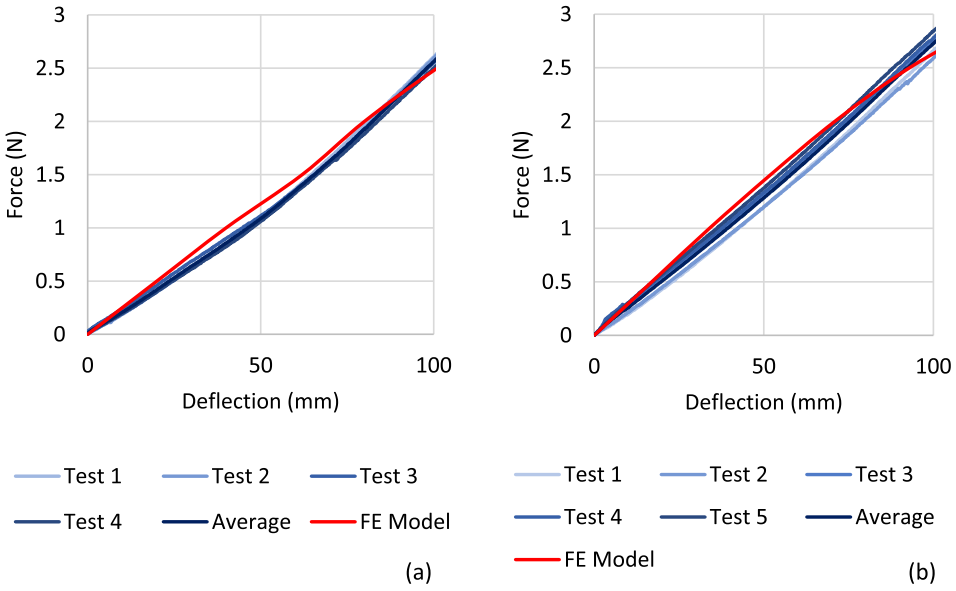

Fig 13. Force/Deflection plot of the eight-strip lattice with only 2 mounting points, comparing the experimental tests to the finite element model (a), Force/ Deflection plot of the new eight-strip lattice (b).

Fig. 14 shows a comparison of the average force/deflection plots of all four experimental configurations and their respective FE models. In general, there is good correlation between all experiments and corresponding FE models. From this plot, the effect of increasing the number of strips and changing the strip configuration is clear. Additional strips, secure mounting and a constant second moment of area result in the conventional eight-strip lattice with all four mounting points secured being the stiffest configuration in this analysis. The second stiffest lattice is the new lattice configuration that also uses eight strips, but only has two mounting points and possesses a sinusoidal variation of second moment of area. The conventional eight-strip lattice using only two mounting points is the next stiffest. The poor mounting conditions create a localised flexibility in the lattice near the root, nullifying the benefit of the constant second moment of area. Finally, the least stiff configuration is the four-strip lattice, with the least strips, only two mounting points and a sinusoidal second moment of area variation in the experiments, together with Eq. (2), created the data displayed in Table 5. With an *EI* of just 555,093 Nmm^2, the four-strip lattice is by far the least stiff lattice in this analysis. Next is the new lattice configuration that has the same stowed height as the four-strip lattice, yet is nearly-three times stiffer with an *EI* of 1,562,251 Nmm^2. The eight-strip lattice with only two mounting points is only slightly stiffer than the new lattice configuration with a *EI* of 1,570,042 Nmm^2. This effect reverses the order shown in Fig. 13, as the new lattice configuration deploys to a slightly shorter length than the other lattices, 560 mm instead of 580 mm. The stiffest lattice in our analysis is the eight-strip lattice

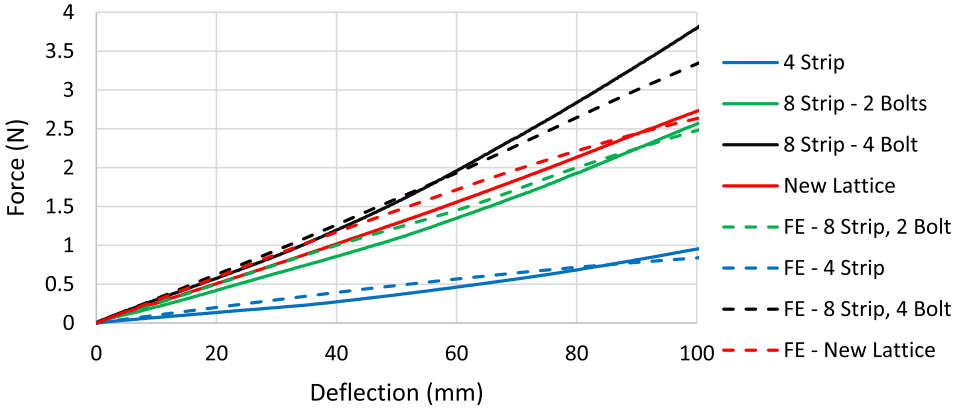

Fig 14. Force/Deflection plot of the four experimental models compared to their respective finite element models.

Table 5
Bending stiffness of the lattices.

Lattice	Mass (g)	Stowed Height (mm)	*EI* (Nmm^2)	*EI* per gram (Nmm^2/g)	*EI* per stowed mm (Nmm)
4-Strip	22.4	50	555,093	24,780	11,101
8-Strip, 2 Bolts	58.9	90	1,570,042	26,656	17,444
8-Strip, 4 Bolts	58.9	90	2,309,435	39,209	25,660
New Lattice	39.2	50	1,562,251	39,853	31,245

The bending stiffness (*EI*) of the lattices was calculated using Eq. (2). The force and deflections recorded.

with all four mounting points, with an *EI* of 2,309,435 Nmm^2, over four times the stiffness of the four-strip lattice. To determine the efficiency of the lattices for use in space deployable structures, two new terms were calculated, *EI* per unit mass and *EI* per stowed mm. Stowed height was used instead of stowed volume as the three lattices have the same stowed radius. These are not usual metrics, but they are useful when considering deployable structures for space applications where bending stiffness, mass and stowed volume are critical design aspects. Using these new terms, it can be determined that the new lattice configuration is the most efficient in terms of mass and stowed volume. The new lattice is only slightly lighter than the fully secured eight-strip lattice, but it is over 20 % more efficient in terms of stowed volume.

6. Conclusion

In this work, a new lattice configuration that uses additional concentrically mounted strips has been developed. These additional strips significantly increase the bending stiffness of the lattice while only marginally increasing both the mass and stowed volume of the structure. A finite element model of the new lattice configuration was developed to calculate the bending stiffness of the structure. This model was then validated through comparison with experimental testing, showing good correlation with a maximum error of 8.5 %. The new lattice configuration was also compared with two conventional lattices, one with the same number of strips and one that stows to the same volume. Compared to the lattice with the same number of strips, the new lattice is 32 % less stiff, but is 33 % lighter and stows to a volume that is 45 % smaller. Compared to the lattice that stows to the same volume, the new lattice is 75 % heavier, but is 281 % stiffer. This work shows that the new lattice configuration is stiffer and more space efficient than the conventional lattice design. This new configuration makes the lattice a more viable option in the design of deployable space structures. By using this type of lattice in the lattice boom structure, straight-line deployment can be achieved, allowing the possibility of using multiple booms in-series in a large solar array.

Funding

The authors would like to thank Science Foundation Ireland for funding the Spatially and Temporally Variable Composite Structures Grant No. (15/RP/2773) under its Research Professor program.

Data availability

Data will be made available on request.

Declaration of Competing Interest

The authors declare that they have no known competing financial interests or personal relationships that could have appeared to influence the work reported in this paper.

References

[1] K. Potter, P.M. Weaver, A.A. Seman, S. Shah, Phenomena in the bifurcation of unsymmetric composite plates, Compos. A Appl. Sci. Manuf. 38 (1) (2007) 100–106.
[2] S. Daynes, P.M. Weaver, Stiffness tailoring using prestress in adaptive composite structures, Compos. Struct. 106 (2013) 282–287.
[3] L.F. Campanile, Initial thoughts on weight penalty effects in shape-adaptable systems, J. Intell. Mater. Syst. Struct. 16 (1) (2005) 47–56.
[4] M. Chamberlain, S. Kiefer, J. Banik, On-Orbit Structural Dynamics Performance of the Roll-Out Solar Array, 2018 AIAA Spacecraft Structures Conference, Kissimmee, Florida, USA, 2018.
[5] B.B. Rennie, New Closed Tubular Extendible Boom, 2nd Aerospace Mechanisms Symposium, Santa Clara, California, 1967.
[6] L. Herbeck, M. Eiden, M. Leipold, C. Sickinger, W. Unckenbold, Development and Test of Deployable Ultra Lightweight CFRP-Booms for a Solar Sail, *European Conference on Spacecraft Structures, Materials, and Mechanical Testing*, Noordwijk, The Netherlands, Noordwijk, The Netherlands, 2000.
[7] K. Seifart, T. Schmidt, W. Göhler, S. Langlois, Structural design of flexible solar generators, Seventh European Space Power Conference, Stresa, Italy, 2005.
[8] J.M. Fernandez, G.K. Rose, C.J. Younger, G.D. Dean, J.E. Warren, O.R. Stohlman, W.K. Wilkie, NASA's Advanced Solar Sail Propulsion System for Low-Cost Deep Space Exploration and Science Missions that Use High Performance Rollable Composite Booms, in: *International Symposium on Solar Sailing*, Kyoto, 2017.
[9] J.M. Fernandez, C.E. Volle, Corrugated Rollable Tubular Booms, AIAA Scitech Forum 2021, Orlando, Florida, 2020.

[10] S. Dubowsky, Dealing with vibrations in the deployment structures of space robotic systems, *Proceedings of the 5th International Conference on Adaptive Structures*, 1994.
[11] E. Groskopfs, Storable tubular extensible member device, US Patent 3434674, 25 03 1969.
[12] J. Banik, S. Kiefer, M. LaPointe, P. LaCorte, On-orbit validation of the roll-out solar array, 2018 IEEE Aerospace Conference, Big Sky, Montana, 2018.
[13] J. Reveles, M. Lawton, V. Fraux, V. Gurusamy, V. Parry, In-Orbit Performance of AstroTube: AlSat Nano's Low Mass Deployable Composite Boom Payload, 31st Annual AIAA/USU Conference on Small Satellites, Logan, Utah, USA, 2017.
[14] T.W. Murphey, J. Banik, Triangular rollable and collapsible boom, United States Of America Patent 7,895,795, 2011.
[15] A. Pirrera, X. Lachenal, S. Daynes, P.M. Weaver, I.V. Chenchiah, Multi-stable cylindrical lattices, J. Mech. Phys. Solids 61 (11) (2013) 2087–2107.
[16] C. McHale, D.A. Hadjiloizi, R. Telford, P.M. Weaver, Morphing composite cylindrical lattices: enhanced modelling and experiments, J. Mech. Phys. Solids 135 (2020) 103779.
[17] C. McHale, S. Carey, D.A. Hadjiloizi, P.M. Weaver, Morphing Composite Cylindrical Lattices: Thermal Effects and Actuation, AIAA Scitech Forum and Exposition, Orlando, Florida, 2020.
[18] C. McHale, R. Telford, P.M. Weaver, Morphing lattice boom for space applications, Compos. Part B: Eng. 202 (2020) 108441.
[19] StructX, Rotated Rectangle - Geometric Properties, StructX, [Online]. Available: https://structx.com/Shape_Formulas_033.html [accessed 09 12 2021].
[20] Engineering ToolBox, Cantilever Beams - Moments and Deflections, 2013. [Online]. Available: https://www.engineeringtoolbox.com/cantilever-beams-d_1848.html [accessed 07 02 2022].
[21] Hibbitt, Karlsson and Sorensen, Abaqus Theory Manual, Version 6.8: Dassault, 2009.
[22] Hexcel Corporation, Hexply 8552 Data Sheet, 2016. [Online]. Available: https://www.hexcel.com/user_area/content_media/raw/HexPly_8552_eu_DataSheet.pdf [accessed 16 October 2019].